A New Test Rig for the Investigation of Film Cooling on Rough Surfaces

Tobias Glasenapp[1]*, Marc Fraas[1], Achmed Schulz [1], Hans-Jörg Bauer[1]

ISROMAC 2017

International Symposium on Transport Phenomena and Dynamics of Rotating Machinery

Maui, Hawaii

December 16-21, 2017

Abstract

This paper describes a new test rig which is designed for the investigation of film cooling on rough surfaces. The cooling holes are geometrically scaled up to increase the measurement resolution. All relevant nondimensional parameters are considered to ensure transferability of the results. Hot gas and coolant temperatures are chosen in a way that the density ratio is close to real engine conditions. The design of the rough test surfaces is based on surface roughness measurements on real turbine blades and scaled matching the nondimensional roughness height k^+. The superposition approach is used for the calculation of local adiabatic film cooling effectiveness and heat transfer coefficients. In-situ calibrated high-resolution infrared thermography is applied for temperature measurements on the test plate. Results of flow measurements of the inlet hot gas flow are shown proving its uniformity. Heat transfer coefficients without film cooling are evaluated and compared to a flat plate correlation confirming functionality of the test rig and data processing methods.

Keywords

Experimental Film Cooling — Heat Transfer — Surface Roughness

[1] *Institute of Thermal Turbomachinery (ITS), Karlsruhe Institute of Technology (KIT), Karlsruhe, Germany*

*__Corresponding author__: tobias.glasenapp@kit.edu

NOMENCLATURE

A_F	Frontal area
A_S	Reference area (without roughness)
A_W	Windward wetted surface
c_f	Skin friction coefficient
D	Cooling hole diameter
DR	Density ratio (= ρ_c/ρ_h)
h	Heat transfer coefficient
H	Thickness
k	Average roughness height
k_s	Equivalent sand grain roughness height
k^+	Nondimensional roughness height
k_s^+	Nondimensional equiv. sand grain roughness height
K	Acceleration parameter
l	Unheated starting length
l_ϵ	Turbulent length scale
L	Cooling hole length
$\dot{m}$	Mass flow rate
M	Blowing ratio (= $(\rho_c u_c)/(\rho_h u_h)$)
Ma	Mach number
Nu	Nusselt number
p	Pressure
P	Cooling hole pitch
Pr	Prandtl number
$\dot{q}$	Specific convective heat flux
Re	Reynolds number
T	Temperature
Tu	Turbulence intensity
u	Free stream velocity
u_τ	Shear velocity
x	Streamwise coordinate
y	Lateral coordinate
z	Wall-normal coordinate

Greek

α	Ejection angle
β	Compound angle
δ	Boundary layer thickness
ϵ	Emissivity
η	Film cooling effectiveness
λ	Thermal conductivity
Λ_s	Combined roughness density and shape parameter
ν	Kinematic viscosity
ρ	Density
σ	Standard deviation
τ_w	Wall shear stress

Subscripts

aw	Adiabatic wall
c	Coolant
dyn	Dynamic
f	Film cooling
IR	Infrared

h	Hot gas
lat	Laterally averaged
rec	Recovery
TC	Thermocouple
t	Total
w	Wall
0	Baseline (without film cooling)

Abbreviations

FEA	Finite element analysis
ITS	Institute of Thermal Turbomachinery
PEEK	Polyether ether kethone
TiAl	Titanium aluminide ($TiAl6V_4$)

INTRODUCTION

Increasing demands for the effectiveness of cooling systems in modern turbo engines require an even deeper understanding of proven cooling concepts such as film cooling. Surface roughness on turbine blades is induced by thermal barrier coatings or arises during operation of the engine. Roughness has a great effect on fluid flow and heat transfer and thus also on film cooling. Particularly convective heat transfer on surfaces with real roughness is still not entirely understood. Computational methods concerning the prediction of heat transfer are still struggling with such complex flow phenomena. Thus, an experimental approach is chosen to investigate the effect of surface roughness on adiabatic film cooling effectiveness and heat transfer. The aim of this paper is to present a new test rig which is designed and built for this purpose.

LITERATURE REVIEW

Film cooling and its influencing parameters have been studied for many years. Geometric parameters as well as flow parameters have been investigated and nondimensional scaling parameters for film cooling studies are known. Both experimental and computational approaches have been chosen to gain even more insight into the flow field and heat transfer. Bogard and Thole [1] summarize the findings in their review paper.

Investigations dealing with film cooling on rough surfaces have been conducted by Goldstein et al. [2], Barlow and Kim [3], Schmidt et al. [4], Schmidt and Bogard [5], Bogard et al. [6], or Rutledge et al. [7]. However, density ratio between hot gas and cooling air did not match realistic values in all studies leading to difficulties when transferring the results to the real engine. Moreover, heat transfer coefficients are not evaluated in all of the studies. Additionally, some of the studies use roughness heights and shapes that differ from roughness found on real turbine components. To the knowledge of the authors, shaped cooling hole geometries have not been investigated in combination with surface roughness. Since this is the state of the art in modern engines, there is a need for further investigations including systematical variation of roughness parameters in order to assess their effect on adiabatic film cooling effectiveness and heat transfer. Thus, a new test rig is presented in this study to facilitate measurements which close this gap.

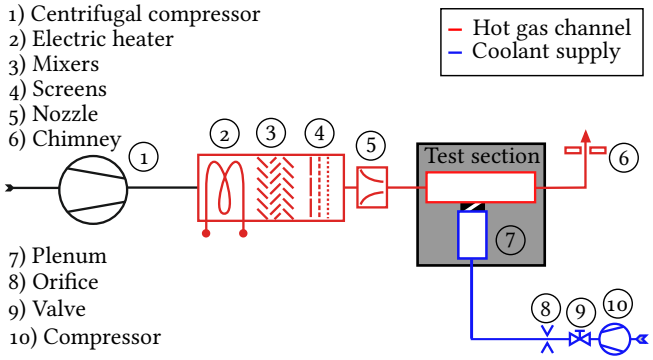

Figure 1. Test facility at ITS including hot gas channel and cooling air supply

EXPERIMENTAL SETUP

The new test rig is designed for generic film cooling studies and is integrated into the test facilities at the Institute of Thermal Turbomachinery (ITS). A schematic of the layout is shown in Figure 1. The hot gas channel is designed as an open loop wind tunnel. Air is provided by a centrifugal compressor ① and heated in an electric heater ② consisting of 40 heating elements that are controlled individually by PID controllers. The flow passes three mixers ③ and several screens ④ for the improvement of the uniformity of temperature and velocity distribution, respectively. The hot air then flows through a nozzle ⑤ which accelerates the flow by a factor of approximately 13 and transfers the circular cross-section in the heater into the rectangular one of the test section.

Cooling air is supplied by a different compressor ⑩. The mass flow rate is controlled by a valve ⑨ and measured with an orifice ⑧. The coolant is fed to a plenum ⑦ from which it enters the test section through the cooling holes.

Test Section

A cross-sectional view of the test section is shown in Figure 2. Hot gas flow enters the test section from the left and is conditioned by a turbulence grid ①. Different turbulence grids can be applied in two different positions in order to adjust the turbulence intensity of the hot gas flow. The grids are designed according to Roach [8] with a porosity greater than 50 % and a minimum distance of 10 mesh lengths to ensure isotropic turbulence at the exit of the cooling holes. A boundary layer bleed ② is placed into the test section in a way that the boundary layer height based on cooling hole diameter is $\delta/D = 0.5$ at the exit of the cooling holes. The position of the boundary bleed is determined using a flat plate correlation for a turbulent boundary layer by Anderson [9].

There are five cooling holes aligned in a row in order to capture coolant jet interaction and to assure periodic conditions for the central hole. All film cooling measurements in

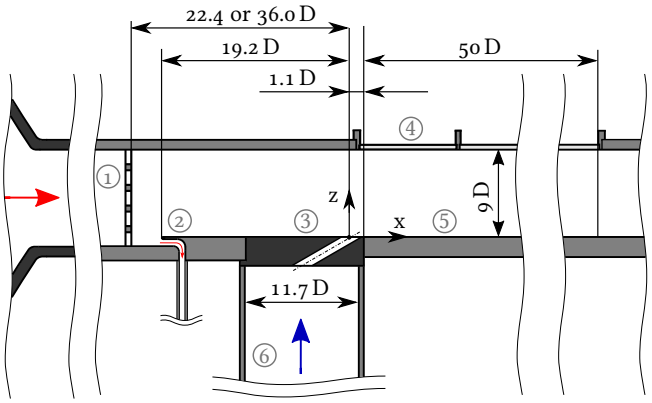

Figure 2. Cross-sectional view of the test section

this study are performed downstream of the central hole in order to exclude wall effects. The holes are geometrically scaled up by a factor of approximately 15-20 in order to increase the measurement resolution. The cooling hole module ③ is interchangeable thus enabling the investigation of different cooling hole geometries. The modules are made of PEEK with a low thermal conductivity of $\lambda_{\mathrm{PEEK}} \approx 0.27\,\mathrm{W\,m^{-1}\,K^{-1}}$. Therefore, heating of the cooling air in the holes is minimized. Cooling hole dimensions are given in Table 1. Future investigations will concentrate on various cooling hole geometries at different lateral spacings.

Based on the study by Fraas et al. [10], the test rig is designed to meet all nondimensional parameters which are relevant for film cooling. During operation of the test rig, these parameters are kept in a range close to real engine conditions to ensure transferability of the results. All test parameters are summarized in Table 2. Temperatures of hot gas and coolant are chosen in a way that realistic density ratios between hot gas and cooling air are achieved. Blowing ratios can be varied over a range typical for real engine applications. Furthermore, acceleration of the hot gas flow can be simulated. The cross-sectional area of the channel is steadily reduced by inclining the top plate. The acceleration parameter K is used as a scaling quantity. The design is based on a calculation of the acceleration through a nozzle considering compressibility of the fluid, but neglecting the boundary layer.

Table 1. Cooling hole dimensions

Parameter	Variable	Value
Length-to-diameter ratio	L/D	6
Pitch-to-diameter ratio	P/D	3…8
Ejection angle	α	30°
Compound angle	β	0°

Table 2. Test parameters

Variable	Value
$Re_{\mathrm{D,h}}$	13000
Ma_{h}	0.11
Tu_{h}	8.3 % or 3.4 %
$l_{\epsilon,h}/D$	0.72 or 0.62
δ/D	0.5
$K = \nu/u^2 du/dx$	≈ 0 or 2×10^{-6}
$DR = \rho_{\mathrm{c}}/\rho_{\mathrm{h}}$	1.7
$M = (\rho_{\mathrm{c}} u_{\mathrm{c}})/(\rho_{\mathrm{h}} u_{\mathrm{h}})$	0.5…3.0

Rough Test Surfaces

McIlroy et al. [11] emphasize the importance of proper scaling roughness height in large-scale laboratory experiments. According to their study, the Reynolds number Re, acceleration parameter K, and nondimensional roughness height

$$k^+ = \frac{u_\tau k}{\nu} \tag{1}$$

need to be met in a test rig, whereas ν represents the kinematic viscosity and u_τ the shear velocity. The geometry of the rough surface needs to match the real roughness. This can be achieved by choosing the appropriate combined roughness density and shape parameter (see Sigal and Danberg [12])

$$\Lambda_{\mathrm{s}} = \frac{A_{\mathrm{S}}}{A_{\mathrm{F}}} \left(\frac{A_{\mathrm{F}}}{A_{\mathrm{W}}} \right)^{-1.6}. \tag{2}$$

The surface areas are shown in Figure 3 (reference area without roughness A_{S}, windward wetted surface A_{W}, and frontal area A_{F}). A recent study by Glasenapp et al. [13] shows detailed measurements of surface roughness on high-pressure turbine vanes. Roughness is evaluated with respect to the three-dimensional surface topography. Amongst other roughness parameters, the combined roughness density and shape parameter Λ_{s} is evaluated. Roughness height is also related to the fluid flow on the turbine blade by calculating corresponding nondimensional roughness heights k^+ and nondimensional equivalent sand grain roughness heights k_{s}^+.

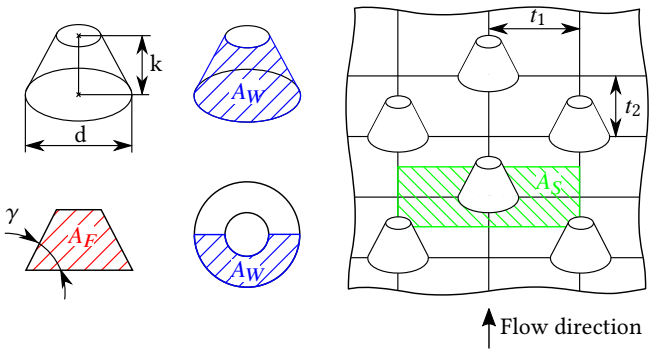

Figure 3. Generic test plate surface roughness consisting of truncated cones

The latter ($k_s^+ = u_\tau k_s/\nu_h$) is chosen as a scaling parameter for the investigation of film cooling on rough surfaces for the test rig presented in this paper. Since temperature and pressure of the hot gas are known, the kinematic viscosity ν_h can be determined. The shear velocity

$$u_\tau = \sqrt{\frac{\tau_w}{\rho}} = u_h\sqrt{\frac{c_f}{2}} \tag{3}$$

of the hot gas flow is calculated using the free stream hot gas velocity u_h and a flat plate correlation for the friction coefficient c_f for turbulent boundary layer flow by Anderson [9]. The shear velocity is calculated at the position of the cooling hole exit assuming a fully turbulent boundary layer without transition. Two different roughness heights $k_s^+ = 20$ and 60 with approximately the same combined roughness density and shape parameter $\Lambda_s \approx 50$ will be investigated. Generic roughness is used on the test plates with truncated cones as roughness elements. Van Rij's correlation $k_s/k = f(\Lambda_s)$ (see van Rij et al. [14]) is used for their design. A schematic of the roughness elements is shown in Figure 3. The rough surfaces are manufactured by milling ensuring high precision of their geometry. Next to the two rough test plates, a hydraulically smooth surface is used as a baseline.

MEASUREMENT TECHNIQUE

This section deals with the measurement techniques that are applied for flow and film cooling measurements as well as the corresponding measurement uncertainties. Figure 4 shows the coordinate system which is used for all measurements presented in this paper. It is placed at the intersection of the axis of the central film cooling hole and the bottom wall of the hot gas channel.

Flow Measurements

The operating point of the test facility is set according to the test parameters described above. Total temperature $T_{t,c}$ and static pressure of the coolant p_c are measured in the plenum $5D$ upstream of the cooling module. Since flow velocity of the coolant in the plenum is below $1\,\mathrm{m\,s^{-1}}$, static pressure and temperature are considered equal to their total quantities. The coolant mass flow rate $\dot{m}_c$ is measured at an orifice farther upstream of the test section. The pipework between point of measuring and cooling holes is tested for leaks to avoid errors. Leakage of coolant mass flow rate is less than 0.3 % for all blowing ratios of interest. A combined total pressure and total temperature probe is placed at position 1 (see Pos.1, Figure 4) at a height of $z/D = 5$ for monitoring the operating point. Hot gas parameters $p_{dyn,h}$, $T_{t,h}$, and p_h are measured continuously. The latter is acquired at a static pressure tap at the top of the channel. From those quantities, the hot gas free stream velocity u_h as well as the hot gas Reynolds number $Re_{D,h}$ are calculated. Based on the coolant quantities, the density ratio DR is set by adjusting the hot gas temperature. The blowing ratio

$$M = \frac{\rho_c u_c}{\rho_h u_h} = \frac{\dot{m}_c}{5A_{hole}\rho_h u_h} \tag{4}$$

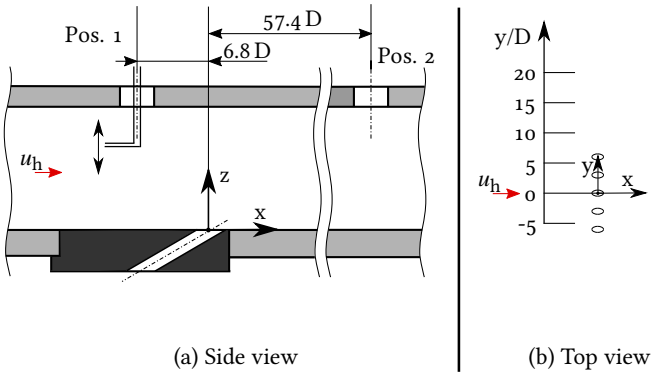

(a) Side view (b) Top view

Figure 4. Measurement positions for operating point and probe measurements

is set by controlling the valve for the coolant supply.

The inlet hot gas flow is investigated in this study in order to verify its uniformity concerning temperature and velocity. All flow measurements are carried out at $Re_{D,h} = 13000$ and the hot gas temperature $T_{t,h}$ which is used for the film cooling measurements. A cooling hole module without cooling holes is used for the flow measurements, i.e. no coolant is introduced into the test section. The turbulence grid for the highest turbulence intensity ($Tu_h = 8.3\,\%$) is placed into the channel. Hot gas flow is not accelerated. For the measurements of velocity and temperature distribution, a second combined total pressure and total temperature probe is used along with a static pressure tap at the top of the channel. The probe is inserted at Pos. 1 upstream of the cooling hole exit, as shown in Figure 4. The tip of the is driven to discrete positions in the wall-normal (z-)direction. At each position, data is acquired with a frequency of 15 Hz and averaged for a duration of 2 s. The distance between those discrete points is chosen to be $0.2D$ in the main flow region and $0.05D$ in the boundary layer. In lateral direction, the probe can be placed at different positions between $y/D = \pm 20$ in step sizes of $5D$ (see Figure 4 (b)). For the flow measurements, the operating point probe is placed in the position downstream of the test plate (see Pos. 2, Figure 4).

The flow velocity u_h is related to the velocity of the reference probe u_{ref}. This leads to the deviation

$$\Delta u_h = \frac{u_h}{u_{ref} - u_{offset}}. \tag{5}$$

Since the reference probe is placed downstream of the measurement probe and the flow is accelerated slightly in the channel, there is an offset u_{offset} between the two measurement positions. The offset is taken for the centerline position for both probes at $y/D = 0$ and $z/D = 5$ and used for all other y/D-positions. The velocity of the reference probe in Equation 5 is determined for each y/D-position. Thus, the measurements at different lateral positions can be compared to each other. Data is processed accordingly for the temperature measurements leading to $\Delta T_{t,h}$.

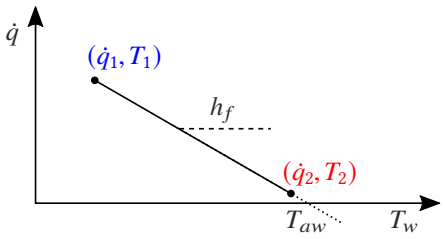

Figure 5. Superposition approach to film cooling

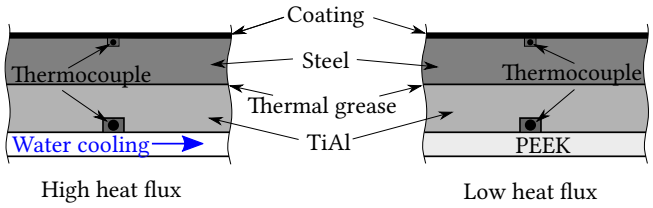

Figure 6. Schematic of the test plate configurations for setting two different thermal boundary conditions

Film Cooling Measurements

Knowledge of local heat transfer coefficients $h_f(x, y)$ and adiabatic film cooling effectiveness

$$\eta_{aw}(x, y) = \frac{T_{rec,h} - T_{aw}(x, y)}{T_{rec,h} - T_{t,c}} \tag{6}$$

is required in order to fully describe a film cooling configuration, whereas $T_{rec,h}$ represents the hot gas recovery temperature, T_{aw} the adiabatic wall temperature, and $T_{t,c}$ the coolant temperature. According to Choe et al. [15], heat transfer on a film-cooled surface can be described by

$$\dot{q}_w(x, y) = h_f(x, y) \cdot \Big(T_{aw}(x, y) - T_w(x, y)\Big). \tag{7}$$

The local specific wall heat flux $\dot{q}_w$ depends on the local heat transfer coefficient h_f as well as on the difference between adiabatic wall temperature T_{aw} and the temperature at the wall T_w. According to Jones [16] it is crucial to match the density ratio DR for a transferability of the heat transfer coefficient h_f. In order to acquire the film cooling quantities in this study, the superposition approach according to Choe et al. [15] is used. It describes the linear relation between wall temperature T_w and heat flux $\dot{q}$ on a film-cooled surface. Figure 5 shows this relation which exists for each point (x,y) on the test plate. The same configuration is measured twice at different thermal boundary conditions on the back side. This way, two different couples of temperature and heat flux are acquired without changing the fluid flow on the surface. Gritsch et al. [17] investigated and confirm the linearity.

In this study, two different test plate configurations are used in order to change the wall heat flux. They are shown in Figure 6. Both are coated with NEXTEL Velvet coating ($\lambda = 0.192\,\mathrm{W\,m^{-1}\,K^{-1}}$, $H \approx 60\,\mu\mathrm{m}$). This finish ensures constant emissivity $\epsilon = 0.94$ of the surface which is almost independent of surface temperature and viewing angle in the range of interest for this study. The test plates consist of three single plates. The top one is made of steel (1.2842, $\lambda = 31.3 - 33.0\,\mathrm{W\,m^{-1}\,K^{-1}}$ in the temperature range of interest, $H = 10.0\,\mathrm{mm}$). Different rough surfaces can be applied by changing the top plate. 0.25 mm type K class 1 thermocouples are glued into small notches as temperature sampling points. The plate in the middle is thermally connected with thermal grease ($\lambda = 3.3\,\mathrm{W\,m^{-1}\,K^{-1}}$) and is made of titanium aluminide (TiAl6V4, $\lambda = 6.5 - 9.8\,\mathrm{W\,m^{-1}\,K^{-1}}$ in the temperature range of interest, $H = 13.6\,\mathrm{mm}$). At its bottom, there are 0.5 mm type K class 1 thermocouples which are glued into notches as well. The bottom plate can be changed for setting the thermal boundary condition which is required for application of the superposition approach. The low heat flux is designed to be close to the adiabatic wall in order to minimize extrapolation error for the adiabatic wall temperature. A thermal insulation made of PEEK is used to realize this in the test rig. The high heat flux is realized by cooling the backside of the test plate with water. Using both points in the diagram (see Figure 5), the slope of the line - which corresponds to the film cooling heat transfer coefficient h_f - is calculated. It is evident that both points need to be as far apart as possible in order to minimize the error which is made when calculating the slope.

Temperatures on the surface of the test plate are measured by in-situ calibrated high-resolution infrared thermography. This measurement technique has been used and further developed at ITS by Ochs et al. [18, 19] and Kneer et al. [20, 21]. Data is processed accordingly in this study. A FLIR SC 6000 infrared camera is used for recording the raw images. A total of five infrared transmissive sapphire windows are embedded into the top wall of the test section. This way the whole surface length of interest is captured with five individual infrared images. Non-uniformity of the infrared camera detector is corrected and the single images are merged using a weighted average in the region where the images overlap. An in-situ calibration is carried out using the 0.25 mm thermocouples which are embedded into the test plate resulting in a high-resolution temperature map of the surface. Since the thermal conductivity of the coating is low, the temperature on top of the coating differs from the one at the thermocouple underneath. Thus, a correction based on the one-dimensional heat flux is implemented to reduce this error. For this correction, the temperature distribution at the bottom of the test plate needs to be known. As shown in Figure 6, at the back side temperatures are measured at discrete locations by thermocouples. They are placed at several positions in streamwise direction. In lateral direction, the thermocouples are placed in the center of the test plate at $y/D = 0$ and at half pitch $P/2$ between the cooling holes. Interpolation both in streamwise direction and lateral direction is carried out in order to receive a temperature distribution of the whole surface.

Both temperature distributions are then fed into a 3D FEA in order to determine the wall-normal heat flux. The FE model ranges from the beginning of the test plate until $50D$ downstream. In lateral direction, the model ranges $P/2$

in both directions. Periodic boundary conditions are set in lateral direction. The conductive wall heat flux is corrected by the radiative heat flux (from the walls of the test rig) in order to get the convective heat flux. After the FE calculation, the temperature distribution on the surface as well as the convective wall heat flux are known. The film cooling quantities are then calculated as follows:

$$T_{\mathrm{aw}}(x,y) = \frac{T_{\mathrm{w},1}\dot{q}_{\mathrm{w},2} - T_{\mathrm{w},2}\dot{q}_{\mathrm{w},1}}{\dot{q}_{\mathrm{w},2} - \dot{q}_{\mathrm{w},1}}, \tag{8}$$

$$h_{\mathrm{f}}(x,y) = \frac{\dot{q}_{\mathrm{w},2} - \dot{q}_{\mathrm{w},1}}{T_{\mathrm{w},1} - T_{\mathrm{w},2}}. \tag{9}$$

Adiabatic film cooling effectiveness is calculated according to Equation 6. The heat transfer coefficient $h_{\mathrm{f}}(x,y)$ is related to the baseline heat transfer coefficient without film cooling

$$h_{\mathrm{o}}(x,y) = \frac{\dot{q}_{\mathrm{w}}}{T_{\mathrm{rec,h}} - T_{\mathrm{w}}} \tag{10}$$

which is measured for each rough test surface, turbulence intensity and acceleration of the hot gas flow.

Measurement Uncertainties

Measurement uncertainties are calculated according to Kline and McClintock [22]. All pressures are acquired by a PSI 9116 Pressure Scanner. Temperature measurements are carried out using thermocouples and a NI SCXI system. 0.5 mm class 1 Type K thermocouples are used for the probe measurements. Their uncertainty is taken from EN 60584-1 [23]. As mentioned earlier, the cooling air mass flow rate is measured with an orifice. Thus, the uncertainty is determined according to ISO 5167-2 [24]. Assumptions for the calculation of the uncertainties are given in Table 3. Measurement uncertainties are given in Table 4. For the heat transfer and film cooling measurements, a steady state of the operating point is awaited. Operating point stability is investigated by averaging operating point quantities and by evaluating standard deviations for the duration of the film cooling measurements.

Table 3. Assumptions used for the calculation of measurement uncertainties

Variable	Uncertainty
Operating Point	
$p_{\mathrm{dyn,h}}$, $\Delta p_{\mathrm{orifice}}$	17 Pa
p_{h}, p_{c}, p_{orifice}	34 Pa
Film Cooling	
$\Delta T_{\mathrm{IR\text{-}TC}}$	1.0 K
$T_{\mathrm{rec,h}}$, $T_{\mathrm{t,c}}$	1.5 K
$\Delta T_{\mathrm{cooled}}$	1.0 K
$\Delta T_{\mathrm{uncooled}}$	1.0 K
H_{Nextel}	10 µm
H_{plate}	0.1 mm
λ	5 %

Table 4. Measurement uncertainties

Variable	Uncertainty
Operating Point	
$Re_{\mathrm{D,h}}$	$\leq$ 1.1 %
u_{h}	$\leq$ 1.0 %
$T_{\mathrm{t,h}}$	$\leq$ 0.3 %
$T_{\mathrm{t,c}}$	$\leq$ 0.5 %
M	$\leq$ 1.7 %
Film Cooling	
h_{f} ($\eta_{\mathrm{aw}} \leq 0.7$)	$\leq$ 12.0 %
η_{aw}	$\leq$ 0.0213

The operating point is very stable with standard deviations amounting $\sigma_{\mathrm{Re}} \leq 0.6\,\%$, $\sigma_{\mathrm{M}} \leq 1.0\,\%$, and $\sigma_{\mathrm{DR}} \leq 0.05\,\%$.

For the calculation of the uncertainties of the film cooling quantities, a procedure according to Fraas et al. [10] is chosen. The heat transfer coefficient is assumed constant at $h_{\mathrm{f}} = 100\,\mathrm{W\,m^{-2}\,K^{-1}}$. For determination of the respective heat flux for the superposition approach, only the temperature difference ΔT between surface and backside temperature is of relevance. Since temperatures are extrapolated from the thermocouples to the plate surface and the thermal conductivity of the coating is low, the coating thickness H_{Nextel} needs to be considered for the uncertainty determination as well. The measurement uncertainties for h_{f} and η_{aw} are given in Table 4.

RESULTS AND DISCUSSION

Results of flow and baseline heat transfer measurements without film cooling are presented in this section. For all measurements, the hydraulically smooth test surface is used as baseline and there is no hot gas flow acceleration.

Flow Measurements

Turbulence intensity is set to $Tu_{\mathrm{h}} = 8.3\,\%$ at the origin of the coordinate system for all flow measurements. Free stream velocity is referenced as described in Equation 5. Deviations of the hot gas flow velocity in wall-normal direction are shown in Figure 7. The profile for the centerline position at $y/D = 0$ looks as expected. At the top wall, the boundary layer is clearly visible and expands approximately over 2 D. At the bottom of the channel, the boundary layer is less distinctive which shows the effect of the boundary layer bleed upstream of the measurement position. Although probe measurements are not suitable for boundary layer measurements, it can be concluded that the boundary layer thickness is in the order of $\delta/D \approx 0.5$ as designed. A different measurement technique will have to be used for boundary layer measurements in a future investigation. Velocity profiles at the same streamwise position at $y/D = \pm 5$ look very similar. There are only small deviations in the free stream region. The largest deviation amounts to approximately 3 %.

For the following figure, boundary layers are cut off and only data of the free stream region in the range of

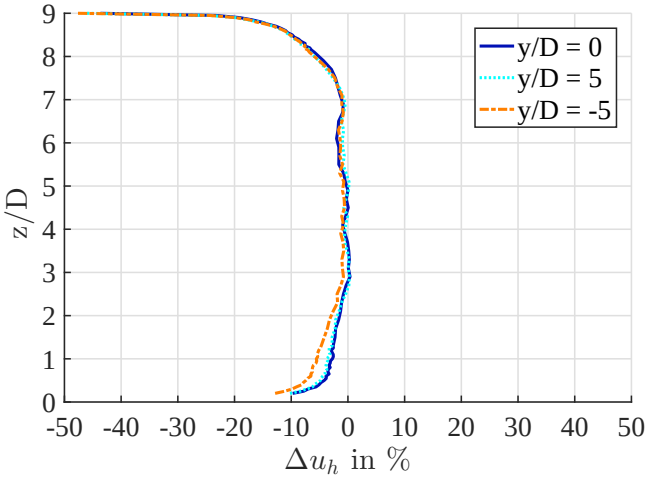

Figure 7. Velocity deviations over the channel height for the centerline ($y/D = 0$) and $y/D = \pm 5$

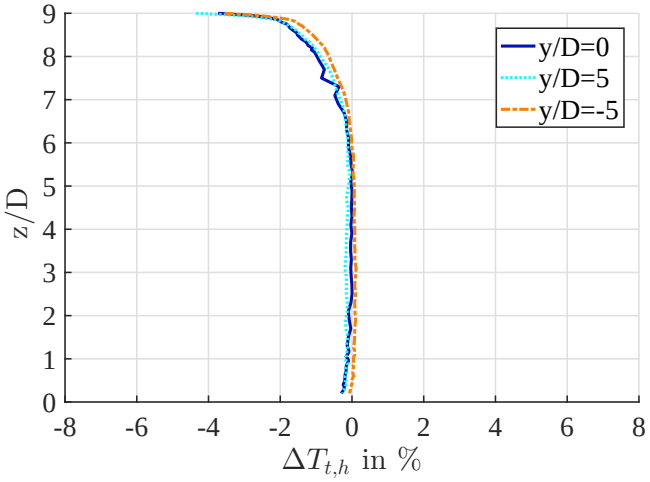

Figure 9. Temperature deviations over the channel height for the centerline ($y/D = 0$) and $y/D = \pm 5$

$1 \leq z/D \leq 7$ is considered. Deviations of the mean velocity Δu_h in the given range is calculated together with the minimum and maximum values. Figure 8 shows deviations of the hot gas flow velocity at discrete y/D positions from $y/D = -20$ to $y/D = 20$ with a step size of 5 D. The flow velocity increases with increasing y/D in the positive y-direction. The distribution of mean values over the channel width in y-direction is very uniform. Deviations in negative y-direction are approximately the same compared to the positive y-direction. However, the deviations are very small even at the positions near the channel wall at $y/D = \pm 20$. The deviations of maximum and minimum values from the mean are less than 3 %. Assuming a maximum cooling hole pitch of $P = 8\,D$, the region of interest for the three central cooling holes is within $-12 \leq y/D \leq 12$. In this region, flow velocity distribution is very uniform.

Temperature profiles of the hot gas flow are shown in Figure 9. The measurements are carried out at the same positions and in the same range as the velocity measurements. As for the flow velocity, the data is referenced by the temperature measured with the probe for monitoring the operating point. The thermal boundary layer at the top of the channel spreads over approximately 3 D. This is beyond the region of region interest for film cooling measurements. At the bottom, the thermal boundary layer is not visible. The temperature distribution is outstandingly uniform. The profiles shown for $y/D = \pm 5$ are in excellent agreement with the one on the centerline at $y/D = 0$. Largest deviations in the free stream region amount less than 0.3 %.

Figure 10 shows the temperature deviations at discrete y/D positions from $y/D = -20$ to $y/D = 20$ with a step size of 5 D. As for the flow velocity, boundary layers are cut off. Data in the free stream region in the range of $1 \leq z/D \leq 6$ is considered. The deviations of maximum and minimum

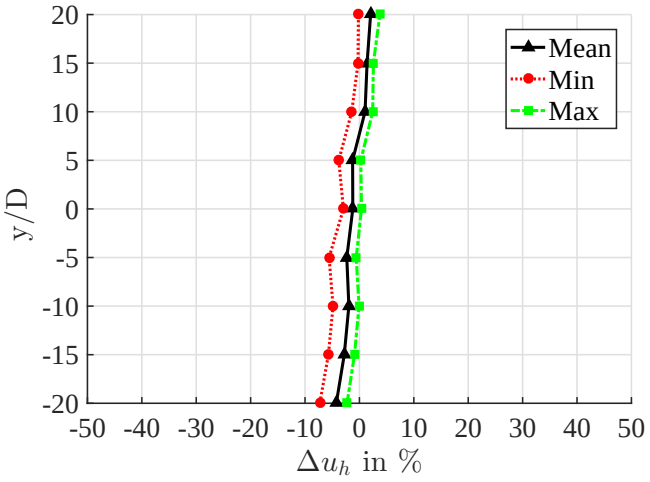

Figure 8. Lateral distribution of hot gas flow velocity deviations for $1 \leq z/D \leq 7$

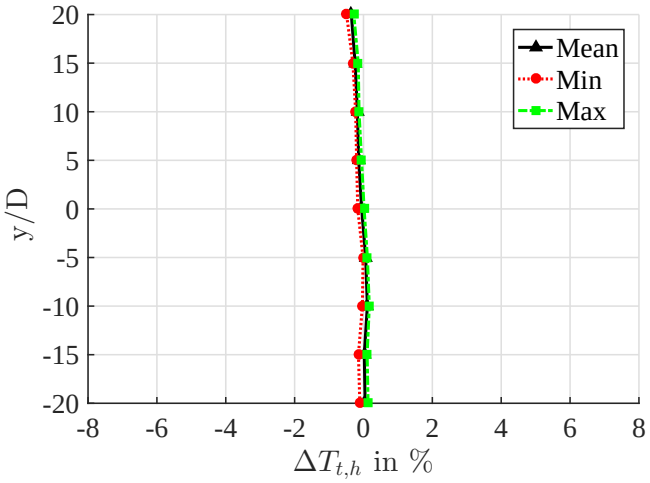

Figure 10. Lateral distribution of hot gas temperature deviations for $1 \leq z/D \leq 6$

values from the mean are very small. The distribution of mean values over the channel width in y-direction is very uniform. Deviations are in the range of measurement uncertainty.

Overall, the inlet flow conditions are very uniform. Thus, high quality film cooling measurements can be carried out in this channel.

Heat Transfer Measurements

Baseline heat transfer measurements are carried out in order to determine the heat transfer coefficients without film cooling $h_o(x, y)$. The measurements are carried out for the high heat flux configuration of the test plate. Corresponding Nusselt numbers $Nu_{x,o} = h_o x/\lambda$ are evaluated and laterally averaged for the surface area on the test plate between $y = \pm 4D$. Figure 11 shows the laterally averaged measurement data of $Nu_{x,o}(x)$ for two different hot gas turbulence intensities $Tu_h = 8.3\,\%$ and $3.4\,\%$, and a flat plate correlation against the Reynolds number $Re_x = u_h x/\nu_h$. Additionally, the x-positions of the cooling hole exit ($x/D = 0$) and the end of the measurement plate ($x/D = 50$) are shown. Since water cooling for the thermal boundary condition is not applied from the beginning of the test plate, but farther downstream, the results are shown for $x/D \geq 5$.

All measurement results show increasing Nusselt numbers with increasing Reynolds number Re_x. Mean deviations for the two different hot gas turbulence intensities $Tu_h = 8.3\,\%$ and $3.4\,\%$ amount approximately $9\,\%$. As expected, higher hot gas turbulence intensity leads to higher Nusselt numbers. Small irregularities for the Nusselt number can be observed at the overlapping areas between the sapphire windows. At the downstream end of the test plate, the slope for the Nusselt numbers increases for both turbulence intensities. This can be attributed to the thermal boundary condition which is set for the FE calculation at this position and will be improved for future data evaluation.

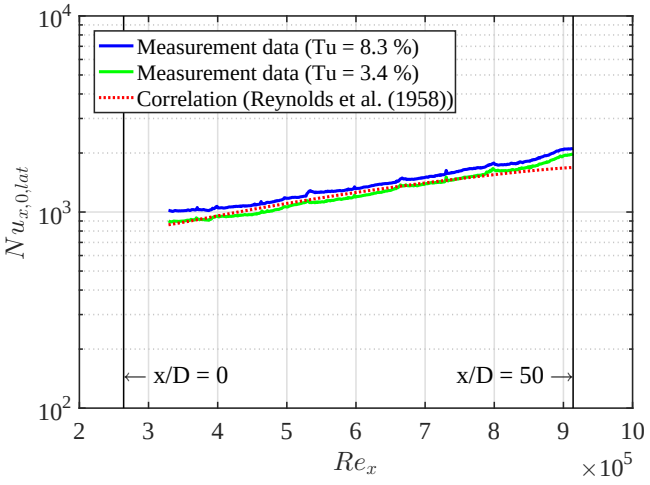

Figure 11. Laterally averaged Nusselt numbers without film cooling $Nu_{x,o}$ against Reynolds number Re_x for the hot gas turbulence intensities $Tu_h = 8.3\,\%$ and $3.4\,\%$, and for a correlation by Reynolds et al. [25]

A correlation for Nusselt numbers on a flat plate by Reynolds et al. [25] is evaluated for validation of the heat transfer data. The test plate in the test rig is cooled strongly in contrast to the parts upstream. This change in thermal boundary condition needs to be considered for the correlation. An adjustment according to Reynolds et al. [25] is used which takes into account the uncooled starting length l. Moreover, the temperatures at the wall of the test plate T_w are low compared to the hot gas temperature $T_{t,h}$. This is taken into account as well. Together with Reynolds number Re_x and Prandtl number Pr, these parameters are inserted into the correlation by Reynolds et al. [25]

$$Nu_x = 0.0296\, Re_x^{0.8} Pr^{0.6} \left[1 - \left(\frac{l}{x}\right)^{0.9}\right]^{-\frac{1}{9}} \left(\frac{T_w}{T_{t,h}}\right)^{-0.4}. \quad (11)$$

Correlation and measurement results are in excellent qualitative and quantitative agreement. Quantitatively, the maximum deviation is less than $15\,\%$ for $x/D \leq 45$. Mean deviation of the correlation from the measurement results is far less amounting approximately $8\,\%$. Altogether, measurement data and correlation are in very good agreement and both heat transfer measurement method and data evaluation are validated.

CONCLUSIONS

A new test rig for the investigation of film cooling on rough surfaces is presented. Cooling holes are scaled up for higher measurement resolution. All relevant nondimensional parameters are met to ensure transferability of the results. Measurement techniques and data processing are discussed and measurement uncertainties are presented.

Inlet hot gas flow is investigated. Extensive measurements of flow and temperature profiles are carried out proving outstanding uniformity of both hot gas flow and temperature distribution. Baseline heat transfer measurements without film cooling are carried out. They are in very good agreement with a flat plate correlation. This demonstrates the functionality of the test rig and data processing methods.

The new test rig is suitable for high-quality film cooling measurements. Different cooling hole shapes as well as hot gas turbulence intensities or flow acceleration can be investigated. More investigations will be carried out in the near future with focus on the effect of surface roughness on local film cooling effectiveness and local heat transfer coefficients.

ACKNOWLEDGMENTS

The investigations were conducted as part of the joint research program COOREFLEX-turbo in the frame of AG Turbo. The work was supported by the Bundesministerium für Wirtschaft und Energie (BMWi) as per resolution of the German Federal Parliament under grant number 03ET7021Q. The authors gratefully acknowledge AG Turbo, MTU Aero Engines AG, Rolls-Royce Germany Ltd & Co KG, and Siemens AG for the support and permission to publish this paper.

Thanks to Benedikt Fischer, Timon Jungh, Steffen Hainz, Lukas Irle, Jonas Müller, Axel Schmid, and Christian Zehnle for their contribution to this paper. The responsibility for the content lies solely with its authors.

REFERENCES

[1] D. G. Bogard and K. A. Thole. Gas Turbine Film Cooling. *Journal of Propulsion and Power*, 22(2):249–270, 2006.

[2] R. J. Goldstein, E. R. G. Eckert, H. D. Chiang, and E. Elovic. Effect of Surface Roughness on Film Cooling Performance. *Journal of Engineering for Gas Turbines and Power*, 107(1):111, 1985.

[3] D. N. Barlow and Y. W. Kim. Effect of Surface Roughness on Local Heat Transfer and Film Cooling Effectiveness. In *Proceedings of ASME Turbo Expo*, 1995. ASME Paper No. 95-GT-014.

[4] D. L. Schmidt, B. Sen, and D. G. Bogard. Effects of Surface Roughness on Film Cooling. In *Proceedings of ASME Turbo Expo*, 1996. ASME Paper No. 96-GT-299.

[5] D. L. Schmidt and D. G. Bogard. Effects of Free-Stream Turbulence and Surface Roughness on Film Cooling. In *Proceedings of ASME Turbo Expo*, 1996. ASME Paper No. 96-GT-462.

[6] D. G. Bogard, D. Snook, and A. Kohli. Rough Surface Effects on Film Cooling of the Suction Side Surface of a Turbine Vane. In *Proceedings of the ASME International Mechanical Engineering Congress and Exposition*, 2003. ASME Paper No. IMECE2003-42061.

[7] J. L. Rutledge, D. Robertson, and D. G. Bogard. Degradation of Film Cooling Performance on a Turbine Vane Suction Side due to Surface Roughness. *Journal of Turbomachinery*, 128(3):547, 2006.

[8] P. E. Roach. The Generation of Nearly Isotropic Turbulence by Means of Grids. *International Journal of Heat and Fluid Flow*, 8(2):82–92, 1987.

[9] J. D. Anderson. *Fundamentals of Aerodynamics*. McGraw-Hill series in aeronautical and aerospace engineering. McGraw-Hill Higher Education, Boston, 4th ed. edition, 2007.

[10] M. Fraas, T. Glasenapp, A. Schulz, and H.-J. Bauer. Introducing a New Test Rig for Film Cooling Measurements with Realistic Hole Inflow Conditions. In *Proceedings of ASME Turbo Expo*, 2017. ASME Paper No. GT2017-63585.

[11] H. M. McIlroy, R. S. Budwig, and D. M. McEligot. Scaling of Turbine Blade Roughness for Model Studies. In *Proceedings of ASME International Mechanical Engineering Congress and Exposition*, 2003. ASME Paper No. IMECE2003-42167.

[12] A. Sigal and J. E. Danberg. New correlation of roughness density effect on the turbulent boundary layer. *AIAA Journal*, 28(3):554–556, 1990.

[13] T. Glasenapp, F. Puetz, A. Schulz, and H.-J. Bauer. Assessment of Real Turbine Blade Roughness Parameters for the Design of a Film Cooling Test Rig. In *Proceedings of ASME Turbo Expo*, 2017. ASME Paper No. GT2017-63088.

[14] J. A. van Rij, B. J. Belnap, and P. M. Ligrani. Analysis and Experiments on Three-Dimensional, Irregular Surface Roughness. *Journal of Fluids Engineering*, 124(3):671–677, 2002.

[15] H. Choe, W. M. Kays, and R. J. Moffat. The Superposition Approach to Film-Cooling. In *Proceedings of ASME Winter Annual Meeting*, 1974.

[16] T. V. Jones. Definition of Heat Transfer Coefficients in the Turbine Situation. In *Turbomachinery, Latest Developments in a Changing Scene*, 1991.

[17] M. Gritsch, S. Baldauf, M. Martiny, A. Schulz, and S. Wittig. The Superposition Approach to Local Heat Transfer Coefficients in High Density Ratio Film Cooling Flows. In *Proceedings of ASME Turbo Expo*, 1999. ASME Paper No. 99-GT-168.

[18] M. Ochs, T. Horbach, A. Schulz, R. Koch, and H.-J. Bauer. A Novel Calibration Method for an Infrared Thermography System Applied to Heat Transfer Experiments. *Measurement Science and Technology*, 20(7):075103, 2009.

[19] M. Ochs, A. Schulz, and H.-J. Bauer. High Dynamic Range Infrared Thermography by Pixelwise Radiometric Self Calibration. *Infrared Physics & Technology*, 53(2):112–119, 2010.

[20] J. Kneer, F. Puetz, A. Schulz, and H.-J. Bauer. Application of the Superposition Principle of Film-Cooling on a Non-Axisymmetric Turbine Endwall. In *15th International Symposium on Transport Phenomena and Dynamics of Rotating Machinery*, 2014.

[21] J. Kneer, F. Puetz, A. Schulz, and H.-J. Bauer. A New Test Facility to Investigate Film Cooling on a Nonaxisymmetric Contoured Turbine Endwall—Part II: Heat Transfer and Film Cooling Measurements. *Journal of Turbomachinery*, 138(7):071004, 2016.

[22] S. J. Kline and F. A. McClintock. Describing Uncertainties in Single-Sample Experiments. *Mechanical Engineering*, 75(1):3–8, 1953.

[23] DIN German Institute for Standardization. Thermocouples - Part 1: EMF Specifications and Tolerances (IEC 60584-1:2013); German Version EN 60584-1:2013, 2014.

[24] DIN German Institute for Standardization. Measurement of Fluid Flow by Means of Pressure Differential Devices Inserted in Circular Cross-Section Conduits Running Full - Part 2: Orifice Plates (ISO 5167-2:2003); German version EN ISO 5167-2:2003, 2004.

[25] W. C. Reynolds, W. M. Kays, and S. J. Kline. Heat Transfer in the Turbulent Incompressible Boundary Layer. Part 2: Step Wall-Temperature Distribution. Technical report, NASA, 1958.